Published in final edited form as:

Cell Rep. 2019 October 29; 29(5): 1057–1065.e4. doi:10.1016/j.celrep.2019.09.057.

HIV-1 Vif Triggers Cell Cycle Arrest by Degrading Cellular PPP2R5 Phospho-regulators

Daniel J. Salamango[1,2,3,*], **Terumasa Ikeda**[1,2,3,4], **Seyed Arad Moghadasi**[1,2,3], **Jiayi Wang**[1,2,3], **Jennifer L. McCann**[1,2,3], **Artur A. Serebrenik**[1,2,3], **Diako Ebrahimi**[1,2,3], **Matthew C. Jarvis**[1,2,3], **William L. Brown**[1,2,3], **Reuben S. Harris**[1,2,3,4,5,*]

[1]Department of Biochemistry, Molecular Biology and Biophysics, University of Minnesota, Minneapolis, MN 55455, USA

[2]Masonic Cancer Center, University of Minnesota, Minneapolis, MN 55455, USA

[3]Institute for Molecular Virology, University of Minnesota, Minneapolis, MN 55455, USA

[4]Howard Hughes Medical Institute, University of Minnesota, Minneapolis, MN 55455, USA

[5]Lead Contact

SUMMARY

HIV-1 Vif hijacks a cellular ubiquitin ligase complex to degrade antiviral APOBEC3 enzymes and PP2A phosphatase regulators (PPP2R5A–E). APOBEC3 counteraction is essential for viral pathogenesis. However, Vif also functions through an unknown mechanism to induce G2 cell cycle arrest. Here, deep mutagenesis is used to define the Vif surface required for PPP2R5 degradation and isolate a panel of separation-of-function mutants (PPP2R5 degradation-deficient and APOBEC3G degradation-proficient). Functional studies with Vif and PPP2R5 mutants were combined to demonstrate that PPP2R5 is, in fact, the target Vif degrades to induce G2 arrest. Pharmacologic and genetic approaches show that direct modulation of PP2A function or depletion of specific PPP2R5 proteins causes an indistinguishable arrest phenotype. Vif function in the cell cycle checkpoint is present in common HIV-1 subtypes worldwide and likely advantageous for viral pathogenesis.

In Brief

Salamango et al. discovered that the HIV-1 accessory protein Vif degrades several PP2A phospho-regulators to induce G2 cell cycle arrest. This activity is prevalent among diverse HIV-1 subtypes

*Correspondence: dsalaman@umn.edu (D.J.S.), rsh@umn.edu (R.S.H.).

AUTHOR CONTRIBUTIONS

D.J.S. and R.S.H. led the project. D.J.S. made all DNA constructs and performed most of the experiments. J.L.M. contributed immunoblots, A.A.S. and S.A.M. to knockdown studies, T.I. and J.W. to cell-based studies, D.E. and M.C.J. to sequence comparisons, and W.L.B. to project logistics. D.J.S. and R.S.H. drafted the manuscript, and all authors contributed to revisions.

DECLARATION OF INTERESTS

R.S.H. is a co-founder, shareholder, and consultant of ApoGen Biotechnologies Inc.

SUPPLEMENTAL INFORMATION

Supplemental Information can be found online at https://doi.org/10.1016/j.celrep.2019.09.057.

and global viral populations, suggesting that virus-induced G2 arrest is advantageous for pathogenesis.

Graphical Abstract

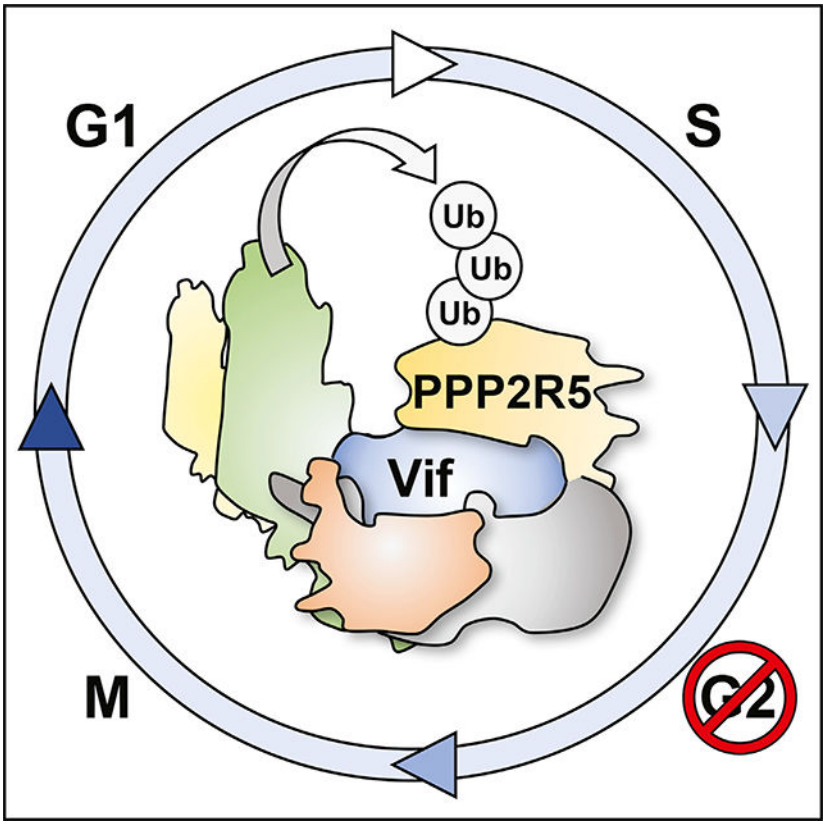

INTRODUCTION

HIV-1 encodes several accessory proteins that are critical for efficient virus replication *in vivo* (reviewed by Harris et al., 2012; Malim and Bieniasz, 2012; Sauter and Kirchhoff, 2018). One of these proteins, Vif, is conserved among primate lentivi-ruses and required for infection in primary $CD4^+$ T cells, macrophages, and many different immortalized cell lines (Gabuzda et al., 1994; Kawamura et al., 1994; von Schwedler et al., 1993). The best-characterized function of Vif is counteracting the restrictive potential of the APOBEC3 family of DNA cytosine deaminases (reviewed by Desimmie et al., 2014; Harris and Dudley, 2015; Malim and Emerman, 2008; Simon et al., 2015). Vif accomplishes this job by heterodimerizing with core binding factor β (CBF-β) and then recruiting Elongin B and Elongin C (ELOB/C), CUL5, and RBX2 to form an E3 ubiquitin ligase complex that polyubiquitinates and degrades restrictive APOBEC3s prior to virus assembly and release (Guo et al., 2014; Jäger et al., 2011). However, in the absence of Vif, APOBEC3G, APOBEC3F, APOBEC3D, and APOBEC3H are capable of packaging into nascent HIV-1 virions and, following entry into a susceptible target cell, physically impede reverse

transcription and catalyze C-to-U mutations in viral cDNA, which can result in G-to-A mutations that render integrated proviral DNA non-infectious.

The only other widely accepted function for HIV-1 Vif is G2 cell cycle arrest (DeHart et al., 2008; Izumi et al., 2010; Sakai et al., 2006; Wang et al., 2007; Zhao et al., 2015). Vif-induced arrest is postulated to involve degradation of an unknown cellular factor because the genetic requirements resemble those for APOBEC3 degradation. For instance, genetic depletion of CBF-β or overexpression of dominant-negative CUL5 both prevent Vif from inducing arrest (Du et al., 2019). Likewise, Vif mutants defective in binding ELOB/C or CUL5 also fail to induce arrest (DeHart et al., 2008). However, the protein surfaces used by Vif for substrate recognition are largely distinct. For instance, comparative analysis between arrest-proficient and -deficient Vif variants revealed several positions essential for inducing G2 arrest that are either fully (APOBEC3G and APOBEC3F) or partially (APOBEC3H) dispensable for APOBEC3 degradation (e.g., positions 31, 33, 36, 48, and 50; Izumi et al., 2010; Zhao et al., 2015). Despite this progress in linking HIV-1 Vif to G2 cell cycle arrest, the precise cellular substrate(s) and overall molecular mechanism(s) have remained elusive.

Quantitative proteomics studies of HIV-1-infected T cells recently revealed Vif-dependent remodeling of the host phosphoproteome and another clue to the G2 arrest mechanism (Greenwood et al., 2016; Naamati et al., 2019). New substrates for Vif degradation have been reported, including members of the PPP2R5 family of protein phosphatase 2A (PP2A) regulators. PP2As function as heterotrimeric complexes that account for a large majority of phosphatase activity in eukaryotic cells (reviewed by Nilsson, 2019; Thompson and Williams, 2018). PP2A trimers are comprised of structural, catalytic, and regulatory (B) subunits. The B subunit can be 1 of 3 distinct protein families (B55, PPP2R5/B56, or PR72/130) that regulate subcellular localization and substrate recognition of holoenzyme complexes (e.g., McCright et al., 1996; Wang et al., 2016). Prior work has linked PPP2R5 regulatory proteins to cell cycle regulation, including the G2-to-M phase transition (reviewed by Moura and Conde, 2019; Nilsson, 2019). However, direct cause-and-effect relationships between Vif, these phospho-regulatory proteins, and G2 cell cycle arrest have yet to be established.

Here a large-scale mutant Vif library is deployed to define the surface used to target PPP2R5 proteins for degradation. A panel of separation-of-function mutants demonstrated that the Vif-PPP2R5 interaction surface is mediated by a conserved network of electrostatic interactions. This comprehensive mutation analysis revealed an inseparable relationship between PPP2R5 degradation and Vif-induced G2 arrest mechanisms. Chemical inhibition of PP2A activity or knockdown of specific combinations of *PPP2R5* transcripts also resulted in similar G2 arrest phenotypes. Functional studies and global bioinformatic analyses both indicated that PPP2R5 degradation and G2 arrest activities are prevalent among diverse HIV-1 subtypes and global viral populations.

RESULTS

Library Construction and Selection Using PPP2R5A as a Vif Substrate

To determine the surface Vif utilizes to degrade the PPP2R5 family of proteins, we generated an ultra-deep mutant library targeting 170 contiguous amino acid positions. The *vif* gene of HIV-1 strain IIIB (identical to NL4–3) was amplified in 6 consecutive segments using sense oligonucleotide primers with a low mutation frequency (~3%) to bias mutations toward single amino acid substitutions (Figure S1A). Individual amplicon libraries were combined by PCR shuffling to generate recombinant products with mutations distributed across all 6 regions. Recombinant amplicons were cloned into a lentiviral transduction vector and subjected to next-generation sequencing (NGS; mutation density is shown in Figure S1B).

The lentiviral vector used for library construction encodes a T2A self-cleaving peptide between mCherry and Vif, which allows efficient detection of transduced cells without having to epitope-tag Vif. To confirm vector functionality, 293T cells stably expressing EGFP-PPP2R5A were transduced with either wild-type IIIB Vif, control vectors, or the mutant library (Figure 1A). Wild-type Vif efficiently degraded EGFP-PPP2R5A whereas the empty vector and $Vif_{SLQ\text{-}AAA}$ did not (the SLQ-AAA mutant fails to engage ELOB/C and does not induce substrate degradation; Larue et al., 2010; Yu et al., 2003). Importantly, library transduction resulted in a high proportion of cells that retained EGFP-PPP2R5A expression (i.e. candidate degradation-defective mutants; Figure 1A, right panel). We chose to screen the library against PPP2R5A because (1) endogenous PPP2R5A is completely degraded by transduction of CEM-T4 cells with HIV-1 (Greenwood et al., 2016; Naamati et al., 2019); (2) PPP2R5A is highly expressed in blood cancer cell lines (Figure 1B); and (3) PPP2R5A localizes to the cytoplasm, where the Vif ligase complex assembles (Figure 1A; McCright et al., 1996). For library screening, EGFP-PPP2R5A cells were transduced at roughly 100× library coverage using a low MOI (<0.1) to ensure that most cells express only a single Vif variant (see schematic in Figure 1C). Transduced cells were subjected to fluorescence-activated cell sorting (FACS) 48 h post-transduction, and populations were separated first by mCherry fluorescence (transduced cells) and then by the presence or absence of EGFP fluorescence (EGFP-PPP2R5A expression or degradation; Figure 1C).

NGS Analysis and Validation of Screening Results

Following FACS, *vif* gene segments were recovered by high-fidelity PCR and subjected to NGS. The sampling frequencies (represented as reads per million [RPM]) were compared between EGFP-positive (non-functional mutant) and EGFP-negative (functional mutant and wild-type) populations to estimate the relative fitness of each Vif mutant (Figure 1D). Three criteria were required for inclusion of a mutant sequence in the final analysis: (1) representation by 15 RPM or more in at least one population, (2) enrichment or depletion value of 2-fold or more, and (3) presence of 3 or more amino acid substitutions. These criteria resulted in 730 Vif mutants with relative fitness ranging from −12 (functional against PPP2R5A) to +10 (non-functional against PPP2R5A) (Figure 1D). Stop codons were enriched at the 5′ end of *vif,* and amino acid substitution mutations occurred throughout.

A total of 10 Vif mutants predicted to either degrade or not degrade EGFP-PPP2R5A were selected for further analysis. Each mutant was transfected into 293T cells stably expressing EGFP-PPP2R5A or APOBEC3G-EGFP (control), and the degradation of each fluorescently tagged target was quantified by flow cytometry. Overall, the degradation phenotypes recapitulated the predictions from the NGS analysis in Figure 1D. For example, R15S, K22T, I31F, R33G, and N48T were predicted to have compromised ability to degrade EGFP-PPP2R5A, and indeed, these substitutions failed to reduce EGFP-PPP2R5A levels compared with wild-type Vif (Figure 1E). Interestingly, all but the K22T substitution could trigger APOBEC3G-EGFP degradation, indicating that the surfaces used to target each substrate are largely distinct. Likewise, L72R, G75T, Q83H, Q105R, and N140Y were predicted to have no effect on degradation, and all reduced both EGFP-PPP2R5A and APOBEC3G-EGFP to levels comparable with those caused by wild-type Vif (Figure 1E). Immunoblots confirmed that all Vif mutants expressed at wild-type levels (Figure S1C).

Defining the Vif Surface Required for PPP2R5 Degradation

To define the surface Vif uses to bind EGFP-PPP2R5A, dedicated degradation studies were done with amino acid substitution mutants that had a relative fitness score of ~1.5 or higher and are surface exposed (Guo et al., 2014). A total of 9 residues fulfilled these two criteria, and 7 of 9 were positively charged lysines or arginines (Figures 2A and 2B; W22 was excluded with a relative fitness score of ~3 because it is not surface exposed). Alanine substitutions at these positions reduced or abrogated Vif's ability to degrade EGFP-PPP2R5A without altering Vif protein expression (Figures 2C and 2D). Moreover, all of these single amino acid substitution mutants could efficiently decrease APOBEC3G-EGFP levels, except for K22A and K26A, which are known to be required for APOBEC3G degradation (Albin et al., 2010; Russell and Pathak, 2007). Taken together, these results strongly indicated that the Vif surface used to bind PPP2R5A is electropositive and genetically separable from the surface used to bind APOBEC3G (i.e., largely-non-overlapping).

PPP2R5 Degradation Is Required for Vif-Mediated Cell Cycle Arrest

Previous studies have suggested that Vif induces G2 arrest by degrading an unknown cellular factor because this process requires the same E3-ubiquitin ligase machinery that is utilized for APOBEC3 degradation (DeHart et al., 2008; Du et al., 2019). We therefore hypothesized that PPP2R5 degradation may, in fact, be the mechanism for Vif-induced G2 arrest. In direct support of this idea, all Vif mutants that failed to degrade eGFP-PPP2R5A were similarly compromised for cell cycle arrest (Figure 2C). Moreover, at least 2 mutants, R23A and K36A, were partially functional for both activities (but not for A3G degradation), further indicating a cause-and-effect relationship. Representative Vif mutants were similarly defective for G2 arrest following expression in the T cell line SupT11 (Figure S2). These data combined support a model in which Vif degrades the PPP2R5 phospho-regulators to induce G2 arrest.

Vif Binds the PPP2R5 Family through Clustered Electrostatic Interactions

We next asked whether Vif uses the same surface to recognize and degrade all 5 PPP2R5 proteins. Previous studies have indicated that Vif can degrade endogenous PPP2R5A/5D and

hemagglutinin (HA)-tagged versions of PPP2R5A–E, but the surfaces and amino acids used to mediate these interactions were not defined (Evans et al., 2018; Greenwood et al., 2016; Naamati et al., 2019). Therefore, a subset of Vif mutants defective in PPP2R5A degradation (above) were transiently expressed in 293T cells stably expressing EGFP-tagged versions of each PPP2R5 family member and analyzed at the single-cell level by flow cytometry. Wild-type Vif degraded EGFP-tagged PPP2R5A–E proteins with variable efficiencies, with 5A being degraded the most and 5E the least (Figure 3A). Several Vif mutants, including K22A, K26A, R33A, and K36A, uniformly failed to reduce the levels of several of the PPP2R5 family members. Importantly, R33A and K36A cannot degrade PPP2R5 proteins but are still capable of promoting wild-type levels of APOBEC3G degradation, making these true separation-of-function mutants (compare PPP2R5 data in Figure 3A and APOBEC3G data in Figure 2C). These results strongly indicated that Vif uses the same surface to recognize and degrade the different PPP2R5 proteins.

Because most amino acids required for PPP2R5 degradation are positively charged, we wondered whether the interface between Vif and the PPP2R5s would be electrostatic in nature. The crystal structure of PPP2R5C supported this idea, with an extensive solvent-exposed surface being overwhelmingly electro-negative (PDB: 2IAE; Wang et al., 2016; Figure S3). Moreover, the other PPP2R5 proteins are homologous (80%–90% similarity) and the predicted structures superimpose with similar electro-negative surfaces (see the PPP2R5A structural model in Figure 3B and comparisons with PPP2R5C in Figure S3). This high degree of structural conservation suggests that this negatively charged surface of the PPP2R5 proteins might be recognized by the positively charged surface of Vif. To directly test this idea, conserved glutamate and aspartate residues were changed to lysine and analyzed by flow cytometry for Vif susceptibility (Figure 3C). This structure-guided mutation analysis revealed PPP2R5A residues that confer complete or partial resistance to Vif-mediated degradation (full resistance: E251, E301, E335, and D338; partial resistance: D205) and strongly implicated this electro-negative patch in binding directly to Vif.

PPP2R5A, 5C, and/or 5D Depletion Induces G2 Arrest Independent of Vif

Although the results above unambiguously linked Vif, PPP2R5 degradation, and G2 cell cycle arrest, it was still unclear which protein (or proteins) must be degraded for this phenotype. To answer this question, we first determined which PPP2R5 proteins are expressed in cell lines that are susceptible to Vif-induced G2 arrest (i.e., 293T, HeLa, SupT11, CEM2n, H9, and THP-1 cells; DeHart et al., 2008; Du et al., 2019; Greenwood et al., 2016; Sakai et al., 2006; Wang et al., 2007; Zhao et al., 2015). qRT-PCR expression data indicated that proteins 5A, 5C, 5D, and 5E are well expressed in these lines, whereas 5B is ~10-fold lower (Figure 4A). These findings were consistent with Cancer Cell Line Encyclopedia (CCLE) RNA sequencing (RNA-seq) data (Figure 1B) and combined suggest that the most likely Vif targets are PPP2R5A, 5C, 5D, and/or 5E (with 5E least favored because of Vif resistance; Figure 3A).

We predicted that short-hairpin RNA (shRNA)-mediated knockdown of the correct Vif target(s) would induce G2 arrest in the absence of Vif. However, although strong *PPP2R5A, 5C, 5D,* and *5E* knockdowns could be achieved in 293T cells, these individual mRNA

depletions had no discernable effect on the cell cycle (Figure 4B). We therefore took a combinatorial knockdown approach and found clear G2 cell cycle arrest phenotypes for 3 different combinations of PPP2R5 proteins (Figure 4C). Strong arrest phenotypes were induced by combining shPPP2R5A and shPPP2R5C, shPPP2R5A and shPPP2R5D, and shPPP2R5C and shPPP2R5D, whereas any combination involving shPPP2R5E showed no effect (Figure 4C). To independently probe whether loss of PP2A function induces G2 arrest, 293T cells were treated with a well-characterized PP2A inhibitor, okadaic acid (Favre et al., 1997; Giese et al., 1995; Ishida et al., 1992), and, interestingly, this compound induced a similarly robust G2 arrest phenotype (Figure 4D). These results demonstrated that at least 2 PPP2R5 proteins must be depleted simultaneously to induce cell cycle arrest and, taken together with the aforementioned data, strongly indicate that Vif induces G2 arrest by degrading the same combination of proteins.

Conservation of the Vif-Mediated PPP2R5 Degradation and G2 Arrest Mechanism

To investigate the mechanistic conservation of this host-pathogen interaction, a panel of viruses from groups M, N, and O was analyzed for G2 arrest, PPP2R5A degradation, and APOBEC3G degradation (see Vif alignments in Figure 5A). As expected from prior studies, all variants could efficiently decrease APOBEC3G-EGFP levels, comparable with HIV-1 IIIB Vif (Figure 5B). In comparison, only group M subtypes B (IIIB), C, and D displayed an ability to degrade EGFP-PPP2R5A and induce G2 arrest, and, in all instances, these two phenotypes were linked. To further confirm this direct relationship, we converted the non-G2-arresting LAI Vif into a G2-arresting derivative by swapping five amino acids in the electro-positive surface region described above to match those in HIV-1 IIIB (Figure 5C).

To further investigate LAI residues involved in PPP2R5 degradation/G2 arrest, the $LAI_{G2\text{-}arrest}$ variant was used to generate a series of reversion mutants (i.e., to systematically exchange IIIB residues back LAI to look for loss of PPP2R5 degradation activity). Surprisingly, reversion of I31V alone nearly abolished EGFP-PPP2R5A degradation (with no effect on APOBEC3G-EGFP degradation), whereas no other single mutants had any effect. Because I31V did not completely abolish EGFP-PPP2R5A degradation, this mutant was combined with additional amino acid substitutions (Figure S4A). Only one double reversion mutant, I31V plus R33G, was able to completely abolish EGFP-PPP2R5A degradation. We further confirmed the importance of positions 31 and 33 by exchanging LAI Vif residues with those of IIIB Vif. Interestingly, exchanging V31I and G33R in LAI Vif together, but not separately, was sufficient to confer EGFP-PPP2R5A degradation activity (Figure S4B). Similar results were obtained with V31I/G33K, demonstrating a requirement for a positive charge at position 33 (Figure S4B and S4C).

We next estimated the proportion of Vif variants in global circulation with the potential to degrade PPP2R5s and induce G2 arrest. Full-length HIV-1 sequences (>8,000 bp) from the Los Alamos database were analyzed when corresponding information was available for subtype and country of sampling (n ~ 2,500). Consistent with previous reports (Buonaguro et al., 2007; Hemelaar et al., 2006), our analyses showed that group M subtype B is the most abundant, circulating in the Americas, Europe, and Australia, whereas group M subtype C is the most abundant in Africa (together, approximately 60% of HIV-1 isolates circulating

globally; Figure 5D). These analyses also indicated that Vif amino acids required for G2 arrest (I31 and R/K33) occur at high frequencies worldwide in subtype B and C HIV-1 isolates (Figure 5D). Taken together with the deep mutation and surface-guided mutation studies above, indicating inextricable roles for these residues in PPP2R5 degradation and G2 arrest, Vif function in PPP2R5 degradation and G2 arrest is likely a contributing factor in the global spread of HIV-1.

DISCUSSION

Although HIV-1 Vif has been intensively studied for its ability to target and degrade the APOBEC3 family of virus restriction factors, its function in G2 cell cycle arrest has been less characterized. Here we show that Vif degrades PP2A phospho-regulators to induce G2 cell cycle arrest. Using deep and structure-guided mutagenesis approaches, the Vif-PPP2R5 interface was mapped to distinct surface regions that are positively and negatively charged, respectively, and likely to interact directly through a network of favorable electrostatics. Vif mutants that were partly or fully defective in PPP2R5 degradation were similarly defective in G2 arrest, suggesting a direct cause-and-effect relationship. This likely molecular mechanism was confirmed by inducing a similar G2 arrest phenotype with pharmacologic inhibition of PP2A function as well as with pairwise genetic depletion of candidate PPP2R5 proteins (independent of Vif). Functional studies and phylogenetic analyses combined indicate mechanistic conservation in roughly half of the global virus population (with HIV-1 subtypes B and C predominating).

Our findings here support a model in which Vif degrades several PPP2R5 family members to activate the G2 checkpoint and create an environment that favors virus replication (Figure S5). PP2A phosphatases have been shown to play at least 3 important roles in the regulation of cell cycle progression from G2 to M phase, and Vif is likely to affect these processes. The first and arguably most critical event for mitotic entry is CDC25-mediated dephosphorylation of CDK1, which activates CDK1 and allows nuclear translocation of the CDK1-CyclinB complex (Lee and Kirschner, 1996; Timofeev et al., 2010). This process is initiated by PP2A/PPP2R5D-catalyzed activation of CDC25 through dephosphorylation, which triggers the release of inhibitory 14–3-3 proteins (Margolis et al., 2006; Figure S5). Thus, Vif-mediated degradation of PPP2R5D would prevent activation of CDC25 and prevent the CDK1-Cyclin B complex from propelling cells into mitosis. In support of this first mechanism, infection of Jurkat T cells with Vif-proficient HIV-1 results in constitutive phosphorylation of CDK1 and concomitant inhibition of CDK1-CyclinB nuclear translocation (Sakai et al., 2011).

Second, PP2A/PPP2R5 complexes also control G2-to-M progression through regulation of the APC-ubiquitin-proteasome complex, which promotes mitotic exit through degradation of specific cellular targets, including Aurora kinases A and B and CDK1-CyclinB (Figure S5). Aurora kinases regulate numerous G2-to-M checkpoints, including spindle assembly, microtubule-kinetochore attachment, and cytokinesis (Fu et al., 2007; Goldenson and Crispino, 2015). In support of this second mechanism, genetic depletion of PP2A/PPP2R5A, 5C, and/or 5D complexes has been shown to result in increased Aurora kinase activity and inhibition of mitotic exit (Foley et al., 2011; Jeong and Yang, 2013). Recent results also

showed that transduction of CEM T4 cells with a Vif-proficient, but not Vif-deficient, virus results in activation of Aurora kinases A/B (Greenwood et al., 2016).

Moreover, a third plausible mechanism is that Vif-mediated degradation of PP2A/PPP2R5A and 5D complexes may also prevent sister chromatid segregation and impede mitotic exit (Figure S5). Loss of PP2A/PPP2R5A/5D results in mislocalization of the centromeric cohesion protector Sgo1 and causes premature chromosomal mis-segregation (Shintomi and Hirano, 2009; Tang et al., 2006). Chromosomal segregation is also negatively affected by constitutive activation of the Aurora kinases (Foley et al., 2011). Taken together, prior studies strongly support a model in which Vif degrades multiple PPP2R5 family members to destabilize multiple independent G2/M checkpoints.

The *vif* gene is conserved in all primate lentiviral lineages and assumed to function predominantly in preservation of viral genomic integrity by degrading APOBEC3 enzymes. However, our results indicate that nearly half of the global viral population may be able to cause PPP2R5 degradation and G2 arrest (Figure 5). Interestingly, HIV-1 Vpr also induces G2 arrest, further suggesting that cell cycle regulation is important for HIV-1 pathogenesis. However, the Vif and Vpr G2 arrest mechanisms are clearly distinct because Vpr requires a different E3-ubiquitin ligase complex (Hrecka et al., 2007). Interestingly, it has been suggested that Vif can delay Vpr-induced G2 arrest by targeting Vpr for proteasomal degradation (Wang et al., 2008). These authors speculated that this mechanism may provide a selective advantage for the virus by delaying G2 arrest and, therefore, the impending cytotoxic phenotype associated with Vpr expression. This model is intriguing because it would result in a longer half-life of an infected T cell, which could lead to an increase in the amount of progeny virions generated during each round of infection. It is also possible that HIV-1 deploys functionally redundant Vif and Vpr mechanisms to achieve greater evolutionary flexibility. For instance, it has been suggested that certain Vif variants have adapted to target APOBEC3H for degradation at the cost of losing G2 arrest activities (Zhao et al., 2015). In this scenario, the virus could still induce G2 arrest through Vpr while simultaneously allowing Vif adaptation.

STAR★METHODS

LEAD CONTACT AND MATERIALS AVAILABILITY

Further information and requests for resources and reagents should be directed to and will be fulfilled by the Lead Contact, Reuben S. Harris (rsh@umn.edu). All constructs generated in this study are all freely available upon request.

EXPERIMENTAL MODEL AND SUBJECT DETAILS

Cell Lines—HEK293T cells were obtained from ATCC (#CRL-3216) and were maintained in DMEM (Hyclone, South Logan, UT) supplemented with 10% FBS (GIBCO, Gaithersburg, MD) and 0.5% pen/strep (50 units). HeLa (#153) and H9 (#87) cells were obtained from the NIH Reagent Program and were maintained in RPMI (Hyclone) supplemented with 10% FBS (GIBCO) and 0.5% pen/strep (50 units). CEM2n (Refsland et al., 2012) and SupT11 (Refsland et al., 2010) cells were generated in the Harris Lab and

were maintained in RPMI (Hyclone) supplemented with 10% FBS (GIBCO) and 0.5% pen/strep (50 units). THP-1 cells were provided by Dr. Andrea Cimarelli (INSERM, France) (Berger et al., 2011) and were maintained in RPMI (Hyclone) supplemented with 10% FBS (GIBCO) and 0.5% pen/strep (50 units)

METHOD DETAILS

Plasmids and Cloning—All expression plasmids used in this study were cloned into the pQCXIH retroviral expression vector (Salamango and Johnson, 2015). The cDNA sequences for all *PPP2R5* genes were ordered as gblocks from Integrated DNA Technologies (IDT) and cloned in-frame with an eGFP coding sequence using *AgeI* and BsiWI restriction sites. The pQCXIH APOBEC3G-eGFP expression vector has been described (Salamango et al., 2018b). PPP2R5A point mutants were generated by PCR amplification using Phusion high fidelity DNA polymerase (NEB, Ipswich, MA) and overlapping PCR to introduce the indicated mutations. All constructs were confirmed by restriction digestion and Sanger sequencing. All oligonucleotide sequences used to generate the constructed used in this study are listed in the Key Resources Table.

Cell Lines and Culture Conditions—293T and HeLa cells were maintained in DMEM (Hyclone, South Logan, UT) supplemented with 10% FBS (GIBCO, Gaithersburg, MD) and 0.5% pen/strep (50 units). SupT11, CEM2n, H9 and THP-1 cells were maintained in RPMI (Hyclone) supplemented with 10% FBS (GIBCO) and 0.5% pen/strep (50 units). The creation and characterization of the SupT11 T cell line has been reported (Refsland et al., 2010). 293T cells were transfected with TransIT LTI (Mirus, Madison, WI) according to the manufacture's protocol. For okadaic acid treatments (Santa Cruz), the indicated concentration was added to the culture medium for 20 hours and then the cells were harvested and subjected to PI staining and flow cytometry to determine DNA content.

To generate stable PPP2R5 and APOBEC3G cell lines, viruses were produced from 293T cells transfected with the pQCXIH retroviral expression vectors described above, an MLV GagPol packaging vector, and a VSV-G vector. Media was harvested 48 hours post-transfection and frozen at −80°C for 4–6 hours, thawed and centrifuged at 1500 × g, and combined with fresh 293T cells. To generate pure cell populations, samples were treated with hygromycin B (Sigma, 200 μg/ml) 48 hours post-transduction.

Library Generation and NGS Analysis—Library synthesis was modified from previous methods (Salamango et al., 2016) and is depicted in Figure S1. Mutagenic oligonucleotide primers were generated by IDT with a mutation frequency of 3% per nucleotide position. These primers were used to amplify IIIB *vif* to produce 6 consecutive mutagenic gene segments. Amplicons were run on an agarose gel and purified (Thermo Fisher gel extraction kit) to ensure each fragment contained only mutagenic segments. Purified DNA fragments were combined in a pseudo-PCR reaction without oligonucleotide primers and cycled for 35 reactions to induce recombination. The reaction product was then diluted 1:40 and added to a PCR reaction containing flanking oligonucleotide primers and cycled for 30 reactions to generate the final library product. The library PCR was run on an agarose gel, purified, digested with *ClaI* and *EcoR*I, and cloned into the indicated lentiviral

expression vector. Bacterial clones were scraped from agar plates and pooled into one culture mix that was grown at 37°C for 3 hours and then DNA plasmid was extracted. Plasmid DNA was PCR amplified with Illumina NGS adaptor primers and subjected to a 2 × 300 bp Miseq run to quantify the number of mutations in the library.

For NGS analysis following library selection, FACS sorted samples were lysed and genomic DNA was extracted and amplified using Illumina NGS adaptor primers. Samples were pooled and subjected to a 2 × 300 bp MiSeq run. Resulting sequence reads were paired, trimmed, and filtered for quality using the FASTx toolkit. Processed reads were translated using EMBOSS and redundant sequences were collapsed and counted into one unique sequence using FASTAptamer (Alam et al., 2015). The functional and nonfunctional sequence files were compared and the resulting enrichment and depletion scores were used to generate the plot in Figure 1D (see text for sequence cutoff criteria).

Cancer Cell Line Expression and HIV-1 Subtype Analysis—Gene expression information for relevant cell lines and tissue types was obtained from the CCLE (https://portals.broadinstitute.org/ccle). Reads per Kilobase per Million (RPKM) values were obtained for available hematopoietic and lymphoid cells lines from the latest CCLE preprocessing pipeline (n = 178). To quality control reads, align/assemble reads to a human reference genome, and quantify individual human gene expression RPKM values (the file CCLE_DepMap_18Q1_RNaseq_RPKM_20180214.gct was used those these analyses). *PPP2R5* gene family mRNA expression was quantified relative to a housekeeping gene, *TBP*. Data were formatted using the statistical analysis software R and RStudio and visualized using the R package ggplot2. For global subtype distributions, full-length HIV-1 sequences were downloaded from http://www.hiv.lanl.govcontent/index (length > 8000bp) with information of HIV-1 subtype and country of sampling. Using one sequence per patient (n~2,500), the distribution of HIV-1 subtypes across the globe was estimated as depicted by region in Figure 5. To identify allelic frequency of specific Vif residues such as positions 31 and 33, sequences were compared to the reference sequence for LAI (accession number K03455).

Quantitative PCR—To determine expression levels of *PPP2R5* transcripts in the panel of cell lines depicted in Figure 4, approximately 250,000 cells were collected and subjected to qPCR analysis. RNA was extracted from the indicated cells using a High Pure RNA Isolation Kit (Roche). Quantification of mRNA was done using primer combinations for the *PPP2R5* family members (qPCR primers used in this study are listed in the Key Resources Table) and the housekeeping gene *TBP* (Burns et al., 2013). All qPCR was done according to the manufacturer recommended protocol on a LightCycler 480 (Roche). For generating stable shRNA knockdown/vector control lines, 293T cells were transfected with the shRNA vector, an HIV-1 Gag/Pol packaging construct, and a VSV-G expression vector. Media was harvested 48 h post-transfection and frozen at −80°C for 4–6 hours, thawed and centrifuged at 1500 × g, and combined with fresh 293T cells. Stable cells either expressed Turbo GFP, and purity was quantified by flow cytometry, or, expressed puromycin resistance and were drug treated for 48 hours to produce a pure population (Sigma, 1 μg/ml).

Cell Cycle Arrest and PP2R5 Degradation Assays—For cell cycle arrest assays, approximately 250,000 293T cells were plated into a 12 well culture plate and allowed to adhere overnight. The next day, cells were transfected with 1 μg of the indicated construct and allowed to incubate overnight. After 24 hours, cells were split into 6 well culture plates and allowed to adhere overnight. At 48 hours post-transfection, cells were detached using PBS/EDTA and centrifuged at 500 × g for 10 minutes. Cell pellets were thoroughly resuspended in 50 μL PBS, mixed with 500 μL cold 70% ethanol, and fixed on ice for 30 minutes. After fixing, cells were centrifuged at 500 × g for 10 minutes and washed twice with PBS. Cell pellets were resuspended in FxCycle PI/RNase staining solution (Invitrogen) for 45 minutes and then analyzed for cell cycle profiling using flow cytometry.

For PPP2R5 degradation assays, cell lines stably expressing either eGFP-PPP2R5A or APOBEC3G-eGFP were plated into 12 well plates at a seeding density of approximately 250,000 cells per well. The next day, cells were transfected with 250 ng of the indicated Vif construct and allowed to incubate for 48 h. After 48 hours post-transfection, cells were harvested using PBS/EDTA and collected for both flow cytometry and immunoblotting to confirm Vif expression. To determine relative eGFP loss, samples were subjected to analysis via flow cytometry. Sample populations were first separated by forward and side scatter to isolate live singular events. After the live/single event population was isolated, the mCherry positive population was isolated and the eGFP fluorescence intensity was assessed. The resulting histograms depicted throughout the manuscript display the eGFP fluorescence profile of the isolated mCherry positive population.

Fluorescence Microscopy Experiments—Approximately 10,000 293T cells stably expressing eGFP-PPP2R5A were plated into a 96-well CellBIND microplate (Corning) and allowed to adhere overnight. The next day, cells were transduced with virus containing the indicated mCh-T2A-Vif variant as indicated in appropriate figure panels and imaged 48 h post transduction. Images were collected at 40x magnification using an EVOS FL Color microscope (ThermoFisher). All images expressing mCherry have been pseudo-colored with magenta instead of red to accommodate readers that may be affected by colorblindness.

Immunoblot Analysis—For immunoblotting assays, the indicated cell line was plated at a seeding density of approximately 250,000 cells per well in a 12 well plate. The next day, cells were either transfected with 250 ng of the indicated Vif construct, or, transduced with the indicated virus and allowed to incubate for 48 h. After 48 hours post-transfection/transduction, cells were collected into 1.5 mL tubes and centrifuged at 500 × g for 10 minutes. Cell pellets were resuspended in 100 mL RIPA buffer (10 μM Tricl-Cl [pH 8.0], 1 mM EDTA, 0.5 mM EGTA, 1% Triton X-100, 0.1% sodium deoxycholate, 0.1% SDS, and 140 mM NaCl) and 10% of the total cell lysate samples were combined with 2.5x SDS-PAGE loading buffer. Samples were separated by a 4%–20% gradient SDS-PAGE gel and transferred to PVDF-FL membranes (Millipore). Membranes were blocked in blocking solution (5% milk + PBS supplemented with 0.1% Tween20) and then incubated with primary antibody diluted in blocking solution. Secondary antibodies were diluted in blocking solution + 0.01% SDS. Membranes were imaged with a LICOR Odyssey instrument or film. Primary antibodies used in these experiments were αActin (Cell

Signaling #4970) and αVif (NIH Reagent Program #6459). Secondary antibodies used were αrabbit IRdye 800CW (LICOR 827–08365), αmouse IRdye 680LT (LICOR 925–68020), αrabbit HRP (Cell Signaling 7074P2), and αmouse HRP (Cell Signaling 7076P2).

QUANTIFICATION AND STATISTICAL ANALYSIS

All flow cytometry data were analyzed using FlowJo 8.8.6 software. The associated histogram profiles of the flow cytometry data in Figures 1, 2, 3, 4, and 5, S2, and S3 were generated using FlowJo 8.8.6 software. The data shown are representative from one of three independent experiments. Bar graphs in Figure 4 and pie charts in Figure 5 were generated using GraphPad Prism 6 software. The "n" values depicted in Figure 5 represent patient Vif sequence data obtained from the Los Alamos database (described above). Protein structures depicted in Figures 2, 3, and S3 were generated using Chimera protein modeling software. Error bars generated for qPCR data in Figure 4 were calculated based on SEM of the data obtained from three independent sample sets.

DATA AND CODE AVAILABILITY

The unique deep sequencing data generated from the Vif library selections used for this study are available at ArrayExpress (E-MTAB-8357). All other materials are available upon request and will be fulfilled by the Lead Contact, Reuben S. Harris (rsh@umn.edu).

Supplementary Material

Refer to Web version on PubMed Central for supplementary material.

ACKNOWLEDGMENTS

This work was supported by NIAID R37 AI064046 (to R.S.H.) and a Collaborative Development Project sub-award from NIGMS 2U54GM103368 and NIAID R21 AI138793 (to D.E.). D.J.S. received salary support from the University of Minnesota Craniofacial Research Training (MinnCResT) program (NIH T90 DE022732) and from a NIAID K99/R00 career transition award (K99 AI147811). R.S.H. is the Margaret Harvey Schering Land Grant Chair for Cancer Research, a Distinguished University McKnight Professor, and an Investigator of the Howard Hughes Medical Institute.

REFERENCES

Alam KK, Chang JL, and Burke DH (2015). FASTAptamer: A bioinformatic toolkit for high-throughput sequence analysis of combinatorial selections. Mol. Ther. Nucleic Acids 4, e230. [PubMed: 25734917]

Albin JS, Haché G, Hultquist JF, Brown WL, and Harris RS (2010). Long-term restriction by APOBEC3F selects human immunodeficiency virus type 1 variants with restored Vif function. J. Virol 84, 10209–10219. [PubMed: 20686027]

Berger G, Durand S, Fargier G, Nguyen XN, Cordeil S, Bouaziz S, Muriaux D, Darlix JL, and Cimarelli A (2011). APOBEC3A is a specific inhibitor of the early phases of HIV-1 infection in myeloid cells. PLoS Pathog. 7, e1002221. [PubMed: 21966267]

Buonaguro L, Tornesello ML, and Buonaguro FM (2007). Human immunodeficiency virus type 1 subtype distribution in the worldwide epidemic: pathogenetic and therapeutic implications. J. Virol 81, 10209–10219. [PubMed: 17634242]

Burns MB, Temiz NA, and Harris RS (2013). Evidence for APOBEC3B mutagenesis in multiple human cancers. Nat. Genet 45, 977–983. [PubMed: 23852168]

DeHart JL, Bosque A, Harris RS, and Planelles V (2008). Human immunodeficiency virus type 1 Vif induces cell cycle delay via recruitment of the same E3 ubiquitin ligase complex that targets APOBEC3 proteins for degradation. J. Virol 82, 9265–9272. [PubMed: 18596088]

Desimmie BA, Delviks-Frankenberrry KA, Burdick RC, Qi D, Izumi T, and Pathak VK (2014). Multiple APOBEC3 restriction factors for HIV-1 and one Vif to rule them all. J. Mol. Biol 426, 1220–1245. [PubMed: 24189052]

Du J, Rui Y, Zheng W, Li P, Kang J, Zhao K, Sun T, and Yu XF (2019). Vif-CBFβ interaction is essential for Vif-induced cell cycle arrest. Biochem. Biophys. Res. Commun 511, 910–915. [PubMed: 30851937]

Evans EL 3rd, Becker JT, Fricke SL, Patel K, and Sherer NM (2018). HIV-1 Vif's capacity to manipulate the cell cycle is species specific. J. Virol 92, e02102–e02117. [PubMed: 29321323]

Favre B, Turowski P, and Hemmings BA (1997). Differential inhibition and posttranslational modification of protein phosphatase 1 and 2A in MCF7 cells treated with calyculin-A, okadaic acid, and tautomycin. J. Biol. Chem 272, 13856–13863. [PubMed: 9153244]

Foley EA, Maldonado M, and Kapoor TM (2011). Formation of stable attachments between kinetochores and microtubules depends on the B56-PP2A phosphatase. Nat. Cell Biol 13, 1265–1271. [PubMed: 21874008]

Fu J, Bian M, Jiang Q, and Zhang C (2007). Roles of Aurora kinases in mitosis and tumorigenesis. Mol. Cancer Res 5, 1–10. [PubMed: 17259342]

Gabuzda DH, Li H, Lawrence K, Vasir BS, Crawford K, and Langhoff E (1994). Essential role of vif in establishing productive HIV-1 infection in peripheral blood T lymphocytes and monocyte/macrophages. J. Acquir. Immune Defic. Syndr 7, 908–915. [PubMed: 7519673]

Giese G, Wiegers W, Kubbies M, Scherbarth A, and Traub P (1995). Okadaic acid Co-induces vimentin expression and cell cycle arrest in MPC-11 mouse plasmacytoma cells. J. Cell. Physiol 163,145–154. [PubMed: 7896891]

Goldenson B, and Crispino JD (2015). The aurora kinases in cell cycle and leukemia. Oncogene 34, 537–545. [PubMed: 24632603]

Greenwood EJ, Matheson NJ, Wals K, van den Boomen DJ, Antrobus R, Williamson JC, and Lehner PJ (2016). Temporal proteomic analysis of HIV infection reveals remodelling of the host phosphoproteome by lentiviral Vif variants. eLife 5, e18296. [PubMed: 27690223]

Guo Y, Dong L, Qiu X, Wang Y, Zhang B, Liu H, Yu Y, Zang Y, Yang M, and Huang Z (2014). Structural basis for hijacking CBF-β and CUL5 E3 ligase complex by HIV-1 Vif. Nature 505, 229–233. [PubMed: 24402281]

Harris RS, and Dudley JP (2015). APOBECs and virus restriction. Virology 479–480, 131–145.

Harris RS, Hultquist JF, and Evans DT (2012). The restriction factors of human immunodeficiency virus. J. Biol. Chem 287, 40875–40883. [PubMed: 23043100]

Hemelaar J, Gouws E, Ghys PD, and Osmanov S (2006). Global and regional distribution of HIV-1 genetic subtypes and recombinants in 2004. AIDS 20, W13–23. [PubMed: 17053344]

Hrecka K, Gierszewska M, Srivastava S, Kozaczkiewicz L, Swanson SK, Florens L, Washburn MP, and Skowronski J (2007). Lentiviral Vpr usurps Cul4-DDB1[VprBP] E3 ubiquitin ligase to modulate cell cycle. Proc. Natl. Acad. Sci. USA 704, 11778–11783.

Ishida Y, Furukawa Y, Decaprio JA, Saito M, and Griffin JD (1992). Treatment of myeloid leukemic cells with the phosphatase inhibitor okadaic acid induces cell cycle arrest at either G1/S or G2/M depending on dose. J. Cell. Physiol 750, 484–492.

Izumi T, lo K, Matsui M, Shirakawa K, Shinohara M, Nagai Y, Kawahara M, Kobayashi M, Kondoh H, Misawa N, et al. (2010). HIV-1 viral infectivity factor interacts with TP53 to induce G2 cell cycle arrest and positively regulateviral replication. Proc. Natl. Acad. Sci. USA 707, 20798–20803.

Jäger S, Kim DY, Hultquist JF, Shindo K, LaRue RS, Kwon E, Li M, Anderson BD, Yen L, Stanley D, et al. (2011). Vif hijacks CBF-β to degrade APOBEC3G and promote HIV-1 infection. Nature 487, 371–375.

Jeong AL, and Yang Y (2013). PP2A function toward mitotic kinases and substrates during the cell cycle. BMB Rep. 46, 289–294. [PubMed: 23790971]

Kawamura M, Ishizaki T, Ishimoto A, Shioda T, Kitamura T, and Adachi A (1994). Growth ability of human immunodeficiency virus type 1 auxiliary gene mutants in primary blood macrophage cultures. J. Gen. Virol 75, 2427–2431. [PubMed: 8077944]

Kelley LA, Mezulis S, Yates CM, Wass MN, and Sternberg MJ (2015). The Phyre2 web portal for protein modeling, prediction and analysis. Nat. Protoc 70, 845–858.

Larue RS, Lengyel J, Jónsson SR, Andrésdóttir V, and Harris RS (2010). Lentiviral Vif degrades the APOBEC3Z3/APOBEC3H protein of its mammalian host and is capable of cross-species activity. J. Virol 84, 8193–8201. [PubMed: 20519393]

Lee TH, and Kirschner MW (1996). An inhibitor of p34cdc2/cyclin B that regulates the G2/M transition in Xenopus extracts. Proc. Natl. Acad. Sci. USA 93, 352–356. [PubMed: 8552637]

Malim MH, and Bieniasz PD (2012). HIV restriction factors and mechanisms of evasion. Cold Spring Harb. Perspect. Med 2, a006940. [PubMed: 22553496]

Malim MH, and Emerman M (2008). HIV-1 accessory proteins–ensuring viral survival in a hostile environment. Cell Host Microbe 3, 388–398. [PubMed: 18541215]

Margolis SS, Perry JA, Forester CM, Nutt LK, Guo Y, Jardim MJ, Thomenius MJ, Freel CD, Darbandi R, Ahn JH, et al. (2006). Role for the PP2A/B56delta phosphatase in regulating 14–3-3 release from Cdc25 to control mitosis. Cell 727, 759–773.

McCright B, Rivers AM, Audlin S, and Virshup DM (1996). The B56family of protein phosphatase 2A (PP2A) regulatory subunits encodes differentiation-induced phosphoproteins that target PP2A to both nucleus and cytoplasm. J. Biol. Chem 277, 22081–22089.

Moura M, and Conde C (2019). Phosphatases in mitosis: roles and regulation. Biomolecules 9, E55. [PubMed: 30736436]

Naamati A, Williamson JC, Greenwood EJ, Marelli S, Lehner PJ, and Matheson NJ (2019). Functional proteomic atlas of HIV infection in primary human CD4+ T cells. eLife 8, e41431. [PubMed: 30857592]

Nilsson J (2019). Protein phosphatases in the regulation of mitosis. J. Cell Biol 278, 395–409.

Pettersen EF, Goddard TD, Huang CC, Couch GS, Greenblatt DM, Meng EC, and Ferrin TE (2004). UCSF Chimera–a visualization system for exploratory research and analysis. J. Comput. Chem 25, 1605–1612. [PubMed: 15264254]

Refsland EW, Stenglein MD, Shindo K, Albin JS, Brown WL, and Harris RS (2010). Quantitative profiling of the full APOBEC3 mRNA repertoire in lymphocytes and tissues: implications for HIV-1 restriction. Nucleic Acids Res. 38, 4274–4284. [PubMed: 20308164]

Refsland EW, Hultquist JF, and Harris RS (2012). Endogenous origins of HIV-1 G-to-A hypermutation and restriction in the nonpermissive T cell line CEM2n. PLoS Pathog. 8, e1002800. [PubMed: 22807680]

Rice P, Longden I, and Bleasby A (2000). EMBOSS: the European Molecular Biology Open Software Suite. Trends Genet. 76, 276–277.

Russell RA, and Pathak VK (2007). Identification of two distinct human immunodeficiency virus type 1 Vif determinants critical for interactions with human APOBEC3G and APOBEC3F. J. Virol 87, 8201–8210.

Sakai K, Dimas J, and Lenardo MJ (2006). The Vif and Vpr accessory proteins independently cause HIV-1-induced T cell cytopathicity and cell cycle arrest. Proc. Natl. Acad. Sci. USA 703, 3369–3374.

Sakai K, Barnitz RA, Chaigne-Delalande B, Bidère N, and Lenardo MJ (2011). Human immunodeficiency virus type 1 Vif causes dysfunction of Cdk1 and CyclinB1: implications for cell cycle arrest. Virol. J 8, 219. [PubMed: 21569376]

Salamango DJ, and Johnson MC (2015). Characterizing the murine leukemia virus envelope glycoprotein membrane-spanning domain for its roles in interface alignment and fusogenicity. J. Virol 89, 12492–12500. [PubMed: 26446598]

Salamango DJ, Alam KK, Burke DH, and Johnson MC (2016). In vivo analysis of infectivity, fusogenicity, and incorporation of a mutagenic viral glycoprotein library reveals determinants for virus incorporation. J. Virol 90, 6502–6514. [PubMed: 27147747]

Salamango DJ, Becker JT, McCann JL, Cheng AZ, Demir Ö, Amaro RE, Brown WL, Shaban NM, and Harris RS (2018a). APOBEC3H subcellular localization determinants define zipcode for targeting HIV-1 for restriction. Mol. Cell. Biol 38, e00356–18. [PubMed: 30224517]

Salamango DJ, McCann JL, Demir Ö, Brown WL, Amaro RE, and Harris RS (2018b). APOBEC3B nuclear localization requires two distinct N-terminal domain surfaces. J. Mol. Biol 430, 2695–2708. [PubMed: 29787764]

Sauter D, and Kirchhoff F (2018). Multilayered and versatile inhibition of cellular antiviral factors by HIV and SIV accessory proteins. Cytokine Growth Factor Rev. 40, 3–12. [PubMed: 29526437]

Shintomi K, and Hirano T (2009). Releasing cohesin from chromosome arms in early mitosis: opposing actions of Wapl-Pds5 and Sgo1. Genes Dev. 23, 2224–2236. [PubMed: 19696148]

Simon V, Bloch N, and Landau NR (2015). Intrinsic host restrictions to HIV-1 and mechanisms of viral escape. Nat. Immunol 76, 546–553.

Tang Z, Shu H, Qi W, Mahmood NA, Mumby MC, and Yu H (2006). PP2A is required for centromeric localization of Sgo1 and proper chromosome segregation. Dev. Cell 70, 575–585.

Thompson JJ, and Williams CS (2018). Protein Phosphatase 2A in the Regulation of Wnt Signaling, Stem Cells, and Cancer. Genes (Basel) 9, E121. [PubMed: 29495399]

Timofeev O, Cizmecioglu O, Settele F, Kempf T, and Hoffmann I (2010). Cdc25 phosphatases are required for timely assembly of CDK1-cyclin B at the G2/M transition. J. Biol. Chem 285, 16978–16990. [PubMed: 20360007]

von Schwedler U, Song J, Aiken C, and Trono D (1993). Vif is crucial for human immunodeficiency virus type 1 proviral DNA synthesis in infected cells. J. Virol 67, 4945–4955. [PubMed: 8331734]

Wang J, Shackelford JM, Casella CR, Shivers DK, Rapaport EL, Liu B, Yu XF, and Finkel TH (2007). The Vif accessory protein alters the cell cycle of human immunodeficiency virus type 1 infected cells. Virology 359, 243–252. [PubMed: 17056089]

Wang J, Shackelford JM, Selliah N, Shivers DK, O'Neill E, Garcia JV, Muthumani K, Weiner D, Yu XF, Gabuzda D, and Finkel TH (2008). The HIV-1 Vif protein mediates degradation of Vpr and reduces Vpr-induced cell cycle arrest. DNA Cell Biol. 27, 267–277. [PubMed: 18462066]

Wang J, Wang Z, Yu T, Yang H, Virshup DM, Kops GJ, Lee SH, Zhou W, Li X, Xu W, and Rao Z (2016). Crystal structure of a PP2A B56-BubR1 complex and its implications for PP2A substrate recruitment and localization. Protein Cell 7, 516–526. [PubMed: 27350047]

Yu X, Yu Y, Liu B, Luo K, Kong W, Mao P, and Yu XF (2003). Induction of APOBEC3G ubiquitination and degradation by an HIV-1 Vif-Cul5-SCF complex. Science 302, 1056–1060. [PubMed: 14564014]

Zhao K, Du J, Rui Y, Zheng W, Kang J, Hou J, Wang K, Zhang W, Simon VA, and Yu XF (2015). Evolutionarily conserved pressure for the existence of distinct G2/M cell cycle arrest and A3H inactivation functions in HIV-1 Vif. Cell Cycle 74, 838–847.

Highlights

- HIV-1 Vif degrades PP2A phospho-regulators to induce G2 cell cycle arrest
- Vif recognizes PP2A regulators through a network of electrostatic interactions
- Combinatorial knockdown studies implicated PPP2R5A, 5C, and 5D in arrest
- Vif-mediated PPP2R5 degradation is conserved in the world's most common subtypes

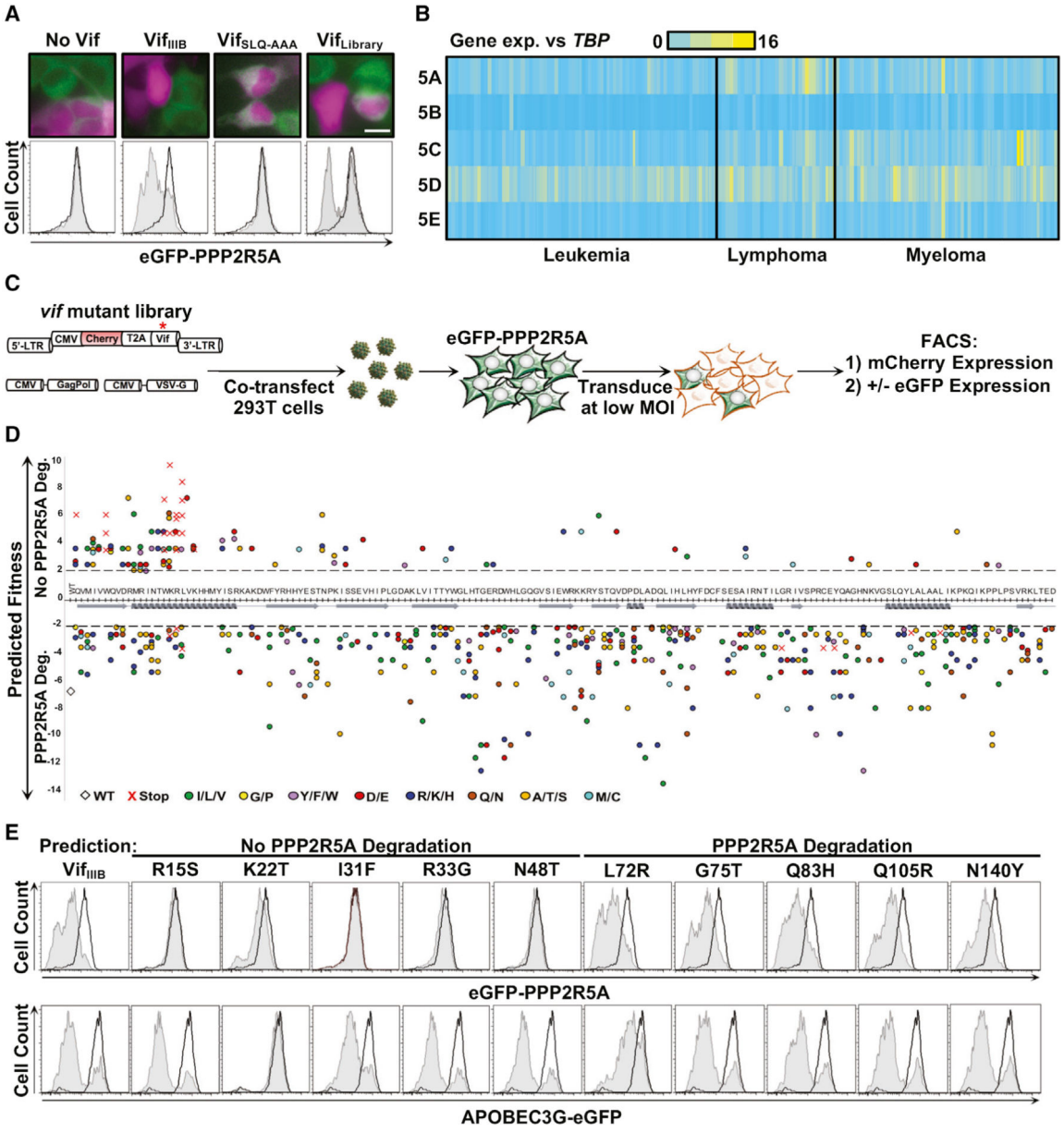

Figure 1. Selection Strategy with NGS Analysis and Validation

(A) Top: representative mCherry and EGFP fluorescence microscopy images of cells stably expressing EGFP-PPP2R5A following transduction of the indicated virus (scale bar, 5 μm). Bottom: flow cytometry histograms of EGFP-PPP2R5A degradation in the presence of the indicated virus (n > 20,000 cells per analysis). The open histogram (black) represents the EGFP profile of cells expressing a degradation-defective Vif mutant (SLQ-AAA), whereas the filled histogram (gray) represents the profile of cells expressing the indicated Vif construct.

(B) Expression profiles of *PPP2R5* family members in the Cancer Cell Line Encyclopedia (n = 178). Expression is shown relative to *TBP* (*TATA-Binding Protein*).

(C) Schematic of the selection strategy used to isolate Vif mutants that either do or do not degrade EGFP-PPP2R5A. See Figure S1 for library construction.

(D) NGS analysis of predicted PPP2R5A degradation-proficient or -deficient Vif mutants recovered from FACS. Each data point represents a substitution, with the corresponding color and symbol indicating the type of substitution.
(E) Single-cell validation of select Vif mutants for their ability to degrade or not degrade EGFP-PPP2R5A or APOBEC3G-EGFP. Histogram profiles are as described in (A) and show representative data from one of three independent experiments.

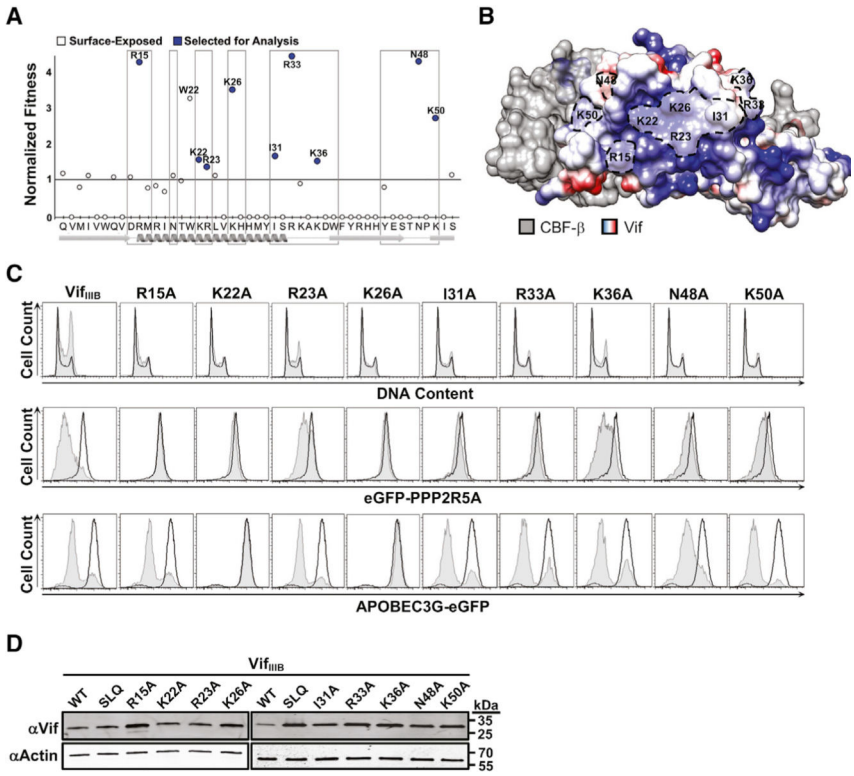

Figure 2. Vif Surface Residues Used to Bind EGFP-PPP2R5A

(A) Depiction of the average fitness scores of Vif amino acid substitutions from positions 5–52. These values were calculated by taking the average enrichment/depletion score at each position for all substitutions identified in Figure 1D. Secondary structures (α helices and β strands) are depicted below the amino acid sequence, with surface-exposed regions outlined by open boxes.

(B) Electrostatic potential map of the residues identified in (A) overlaid on the crystal structure of Vif (PDB: 4N9F).

(C) The top panels show the DNA content of 293T cells transiently expressing the indicated Vif constructs (left peak, G_0/G_1; right peak, G_2). The center and bottom panels report EGFP fluorescence of 293T cells stably expressing either EGFP-PPP2R5A or APOBEC3G-EGFP and transiently expressing the indicated Vif construct. Histogram profiles are as described in Figure 1A and show representative data from one of three independent experiments.

(D) Immunoblots of Vif variants transiently expressed in 293T cells stably expressing EGFP-PPP2R5A. Actin is shown as a loading control.

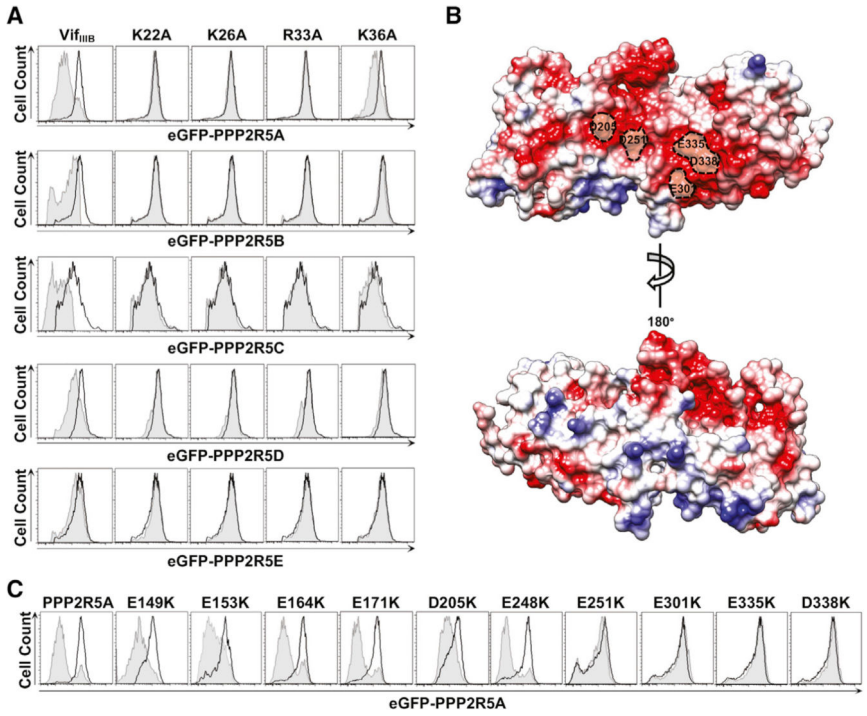

Figure 3. Vif Recognizes the PPP2R5 Family through Electrostatic Interactions

(A) Flow cytometry profiles of EGFP-PPP2R5A–E fluorescence in 293T cells transiently expressing the indicated Vif construct. Histogram profiles are as described in Figure 1A and show representative data from one of three independent experiments.

(B) Electrostatic potential map of a PPP2R5A model structure (based on the PPP2R5C X-ray structure; Figure S2). Labeled residues are required for Vif recognition.

(C) Flow cytometry profiles of 293T cells stably expressing the indicated EGFP-PPP2R5A mutant and transiently expressing HIV-1 Vif (IIIB). Histogram profiles are as described in Figure 1A and show representative data from one of three independent experiments.

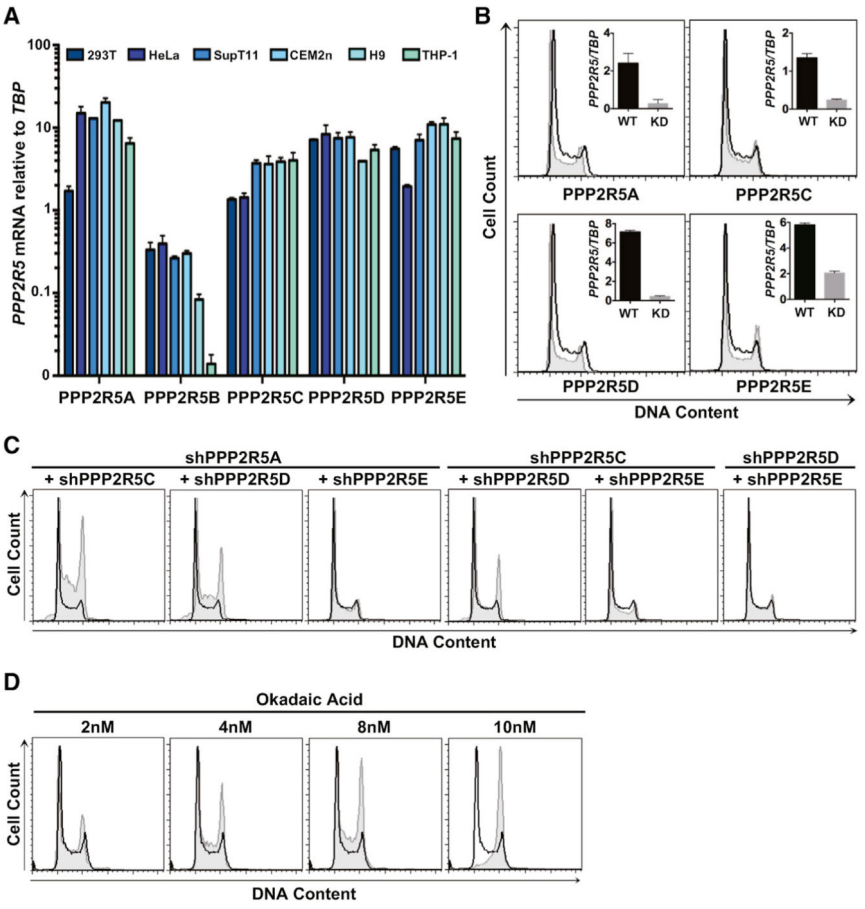

Figure 4. Combinations of PPP2R5A, 5C, and/or 5D Knockdown Induce G2 Arrest in the Absence of Vif

(A) Histogram showing qRT-PCR data for each *PPP2R5* isoform mRNA in the indicated cell lines. Expression values are shown relative to *TBP* and are an average of three independent experiments.

(B) Cell cycle profiles of 293T cells stably expressing either a control shRNA or a shRNA targeting the indicated *PPP2R5* transcript. Knockdown efficiencies are depicted in the inset relative to *TBP*.

(C) The DNA content of 293T cells stably expressing either control shRNA or the indicated shRNA constructs from (B) (left peak, G_0/G_1; right peak, G_2).

(D) DNA content of 293T cells treated for 20 h with the indicated concentrations of okadaic acid.

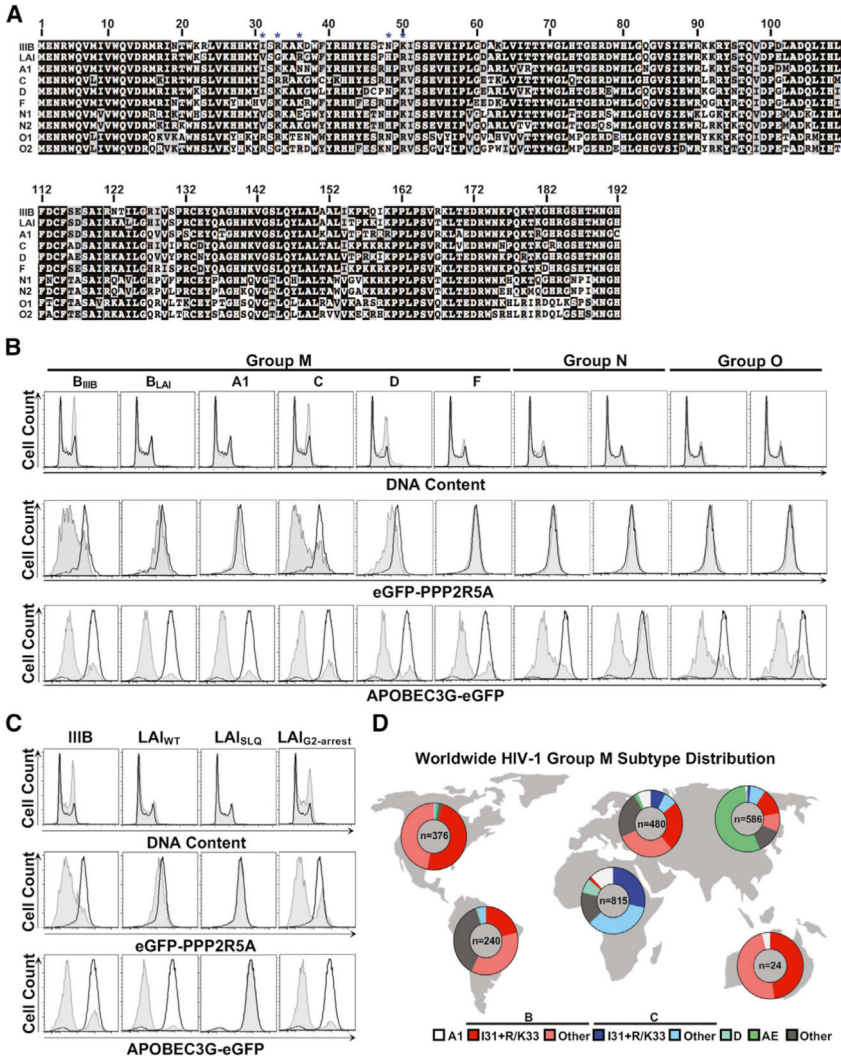

Figure 5. Vif Residues 31 and 33 are Critical for Inducing PPP2R5A Degradation

(A) Amino acid alignment of the HIV-1 Vif variants tested for G2 arrest, PPP2R5A degradation, and APOBEC3G degradation. Blue asterisks indicate the five amino acid residues exchanged in LAI Vif to generate the $LAI_{G2\text{-}arrest}$ variant.

(B and C) Flow cytometry profiles of cells transiently expressing Vif from the indicated HIV-1 subtype (B) or from the indicated lab adapted strain (C). Histogram profiles show the DNA content (top), degradation profiles of 293T cells stably expressing EGFP-PPP2R5A (middle), or APOBEC3G-EGFP (bottom). Histogram profiles are as described in Figure 1A and show representative data from one of three independent experiments.

(D) Global distribution of HIV-1 group M subtypes depicted by pie graphs. Subtypes B and C are also divided by amino acid identity at positions 31 and 33.

KEY RESOURCES TABLE

REAGENT or RESOURCE	SOURCE	IDENTIFIER
Antibodies		
αVif	NIH Reagent Program	#6459
αActin	Cell Signaling	#4970; RRID: AB_2223172
αrabbit IRdye 800CW	LICOR	#827–08365; RRID: AB_10796098
αmouse IRdye 680LT	LICOR	#925–68020; RRID: AB_2687826
αrabbit HRP	Cell Signaling	#7074P2; RRID: AB_2099233
αmouse HRP	Cell Signaling	#7076P2; RRID: AB_330924
Bacterial and Virus Strains		
E. coli DH10B	Harris Lab Collection	N/A
E. coli 5-alpha electrocompetent	NEB	C2989K
HIV_{IIIB} Vif/VprXX provirus plasmid	Salamango et al., 2018a	N/A
Critical Commercial Assays		
FxCycle PI/RNase Staining	Invitrogen	F10797
Deposited Data		
Illumina MiSeq Data	ArrayExpress	E-MTAB-8357
Experimental Models: Cell Lines		
HEK293T	ATCC	#CRL-3216
HeLa	NIH Reagent Program	#153
Cem2n	Refsland et al., 2012	N/A
SupT11	Refsland et al., 2010	N/A
THP-1	Berger et al., 2011	N/A
H9	NIH Reagent Program	#87
Oligonucleotides		
All oligonucleotide sequences used in this study are provided in Table S1	This paper	Table S1
Recombinant DNA		
All recombinant DNA used in this study are listed in Table S2	This paper	Table S2
Software and Algorithms		
UCSF Chimera	Pettersen et al., 2004	http://www.cgl.ucsf.edu/chimera/
Phyre2 Protein Fold Recognition Server	Kelley et al., 2015	http://www.sbg.bio.ic.ac.uk./html/page.cgi?id=index
FASTX-Toolkit	N/A	N/A
EMBOSS-Transeq	Rice et al., 2000	http://emboss.sourceforge.net/
FASTAptamer	Alam et al., 2015	https://www.burkelab.missouri.edu/fastaptamer.html
Statistical analysis software R and RStudio	N/A	http://www.r-project.org
FlowJo 8.8.6	N/A	https://www.flowjo.com/
GraphPad Prism 6	N/A	https://www.graphpad.com/
Other		

REAGENT or RESOURCE	SOURCE	IDENTIFIER
CellBind 96 well microplate	Corning	#CLS3340
TransIT LTI transfection reagent	Mirus Bio	#MIR2306
EVOS FL Color microscope	Thermo Fisher Scientific	#AMEFC4300
BD FACSCanto II Flow Cytometer	BD Biosystems	N/A